Earthq Eng & Eng Vib (2023) 22: 703-718 **DOI**: https://doi.org/10.1007/s11803-023-2194-8

Earthquake response of wrap faced embankment on soft clay soil in Bangladesh

Ripon Hore[1†], Sudipta Chakraborty[2‡], Kamruzzaman Kamrul[3§], Ayaz Mahmud Shuvon[4*] and Mehedi A. Ansary[5£]

1. *LGED, Dhaka, Bangladesh*
2. *Kongju National University, Cheonan, South Korea*
3. *Department of Civil Engineering, Bangladesh University of Engineering, Dhaka, Bangladesh*
4. *Bangladesh Network Office for Urban Safety* (*BNUS*)*, Bangladesh University of Engineering and Technology, Dhaka, Bangladesh*
5. *Department of Civil Engineering, Bangladesh University of Engineering and Technology, Dhaka, Bangladesh*

Abstract: A wrap-faced embankment model on soft clay soil subjected to earthquake motion was investigated in this study. The study was conducted both experimentally using a shaking table and numerically using PLAXIS 3D software. The amplification of acceleration, displacement, pore water pressure, and strain response were measured while varying input accelerations and surcharge pressures. Time histories of the Kobe record of the 1995 Hanshin earthquake were used as the input seismic motion. The input acceleration was 0.05 g, 0.1 g, 0.15 g, and 0.2 g, and different surcharge pressures were 0.70 kPa, 1.12 kPa, and 1.72 kPa with relative density of Sylhet sand fixed to 48%. The output data from the shaking table tests and the numerical analysis performed through the PLAXIS 3D software were compared, and these findings were also compared with some earlier similar studies. The acceleration amplification, displacement, pore water pressure, and strain (%) changed along the elevation of the embankment and acceleration response increased with the increase in base acceleration. The increase was more noticeable at higher elevations. These findings enrich the knowledge of predicting the dynamic behavior of wrap-faced embankments and enable the design parameters to be adjusted more accurately.

Keywords: shaking table test; soft clayey soil; kobe earthquake; seismic wave; wrap-faced soil embankment

1 Introduction

Highway embankments and different types of earth structures should be stable enough, so that they can withstand the ground motions during and after an earthquake to provide safety. In earthquake engineering, the foundation of clayey soil has been an area of great focus. Studying the behavior and the characteristics of displacement, strain, and pore water pressure when subjected to seismic waves is often a complicated and tedious process. Pore water pressure may rise when subjected to a seismic load, which may subsequently cause a drop in effective stress and then to softening of soil. This softening of soil may cause damage to the structure. In this case, to achieve structural stability, engineering interventions are necessary to reinforce the embankment. Geosynthetics have the capacity to absorb energy and emit less energy to the structure, which is an economical approach to alleviate the earthquake intensity on the geo-structure (Yegian *et al*., 1999; Edinçliler and Güler, 1999). Due to its performance under seismic loading and cost-effectiveness, many scholars (Sakaguchi *et al*., 1992; Sakaguchi, 1996; Huang and Wang, 2005) have studied reinforced soil retaining walls.

There are many ways to determine the seismic response of soil with reinforcement. These are experimental, analytical, and numerical model studies. The first one is experimental studies, which are mostly based on shake table tests and centrifuge tests. Washida and Shimazu (1988) observed the effect of seismic motion of the reinforced embankment by shake table tests. Later Perez and Holtz (2004), Latha and Krishna (2008) and Turan *et al*. (2009) investigated and conducted extensive research in this field. The seismic effects were recorded and the findings of their study were published regarding reinforced soil slopes, different models of retaining walls, and laminar containers for soil. Also, along with the shake table tests, Nova-Roessig and Sitar (2006) and Viswanadham *et al*. (2009) developed a centrifuge model which they used to investigate seismic effects and published the findings of their study. Chakraborty *et al*. (2021a) investigated the dynamic behavior of a wrap-faced embankment on soft clay using shake table tests.

Correspondence to: Ripon Hore, Senior Assistant Engineer, LGED, Dhaka, Bangladesh
Tel: +880-1711573363
E-mail: riponhore@gmail.com
[†]Senior Assistant Engineer; [‡]Master Student; [§]Post Graduate Student; [*]Research Assistant; [£]Professor

Received July 25, 2021; **Accepted** September 11, 2022

They used sinusoidal waves for dynamic input motion. Regarding the analytical model studies, this literature primarily provides an approximate infusion to the actual dynamic nature by using the pseudo-static analytical value. Choudhury *et al*. (2006) conducted experiments and revealed findings with a comparison of seismic reactions on retaining walls.

The final method is the computational numerical method. Using finite element method-based software, a prototype structure is modeled first. This is usually used when the prototype structure is inconvenient to test in a lab. In this method, a model is first developed and then calibrated by data from earlier experiments. The disparity between the prototype and the model is adjusted to remove the differences. Then this calibrated model can be used in extensive studies. These advantages make numerical modeling better for regular use. Bhattacharjee and Krishna (2013) used FLAC 3D to analyze the behavior of the model soil walls. Wulandari and Tjandra (2015) predicted the optimum tensile strength of geotextile with PLAXIS 2D. This validation and calibrations are done with the strains, displacements, and settlement parameters. Hore *et al*. (2021) recorded and studied the seismic effects of wrap-faced embankment on soft clay subjected to sinusoidal waves in both experimental and numerical analysis. Sakaguchi *et al*. (1992, 1996) and Lu *et al*. (2018) carried out a shaking table test. The height of the prototype was 1.5 m upon which effects on different parameters are recorded and analyzed when subjected to seismic waves. Improvement of ground is another more economical way, which improves the seismic resistance of existing subsurface structures.

Reinforced soil or mechanically stabilized structures are used nowadays as a substitute to conventional earth-retaining structures due to their better performance. They provide a result in the perspective of the pace of construction, volume, and loading limit. Several researchers stated and reached a unified conclusion that reinforced soils perform better than conventional earth retaining structures (e.g., Tatsuoka *et al*., 1997; Koeski *et al*., 2006; Huang *et al*., 2018; Zhou *et al*., 2020; Mohanty *et al*., 2021; Damians *et al*., 2021; Zhang *et al*., 2022; Pan *et al*., 2022; Hore *et al*., 2022).

Moreover, Krishna and Bhattacharjee (2017, 2019) demonstrated the development of a calibrated model and analyzed the input ground motions at the bottom of the rigid-faced reinforced soil-retaining wall and their response at the top. Huang (2019) studied and published the findings after analyzing the effect of a seismic wave on a 0.6 m vertical wrap-around reinforced soil wall. The study showed that the maximum tensile force increases with the depth of the reinforcement. Usually, the tensile forces shape up to an inverted trapezoidal form, but in this case, it generates a trapezoidal shape.

Cengiz and Guler (2018) experimentally determined the performance of geosynthetic enclosed stone columns and regular stone columns implanted in soft clay under dynamic base loading. Gidday and Mittal (2020) conducted a series of shake table tests with geotextile reinforced wrap-faced soil walls and found that the settlement of the vertical crest and horizontal displacement of reinforced soil walls decreases with the number of reinforced layers. Their experiment was conducted with both cement-treated and untreated clay soils, and PLAXIS 3D software was used for numerical modeling with a sinusoidal shaking of 20 cycles.

Different research studies on the dynamic analysis of wrap around embankments used various soil parameters according to local conditions. In this research, dynamic soil properties analysis of the wrap faced embankment considered Bangladeshi soft clayey soil. There are several research studies on stability of the embankment. The stability of the embankment in soft clay soil in Bangladesh with respect to earthquake loading is rare. In the present research, an earthquake resistant wrap faced embankment on soft clay soil has been analyzed by experimental and numerical methods. The target of this study is to determine the outcomes and find the relations among different input earthquake motions with a varying surcharge load, and different accelerations for the Kobe earthquake loading. In total, six independent tests were carried out using the shake table for this particular model embankment. When designing roadway or railway embankment, it is essential to account for the seismic loading. Accounting for the technical parameters and laboratory facilities, a geosynthetic wrap-faced embankment was developed. The effect of acceleration, acceleration amplification, displacement, excess pore water pressure, and strain on the model wall was studied based on the earthquake input motion. In the current research, numerical analysis was also conducted by using PLAXIS 3D to compare with the experimental data.

2 Objectives, goals and location of the study

The objectives of this research are to (a) prepare a model of wrap faced embankment on soft clay, (b) collect the data from experimental shaking table tests, (c) calculate the results from a numerical model using PLAXIS 3D, (d) determine the effects on pore water pressure, displacement, strain, and acceleration amplification for different earthquake (Kobe) input motion, and (e) analyze and compare both experimental and numerical results.

The goal of the research is to invent a type of embankment which has excellent resistance to earthquakes similar to the Kobe event after analyzing the dynamic behavior of soil by experimental and numerical analysis. Sediment deposits are not evenly distributed throughout the country (Hore *et al*., 2019). The major portion of the soil in Dhaka which is the capital of Bangladesh, is soft clay soil. The sample was collected from the Bangladesh University of Engineering (BUET) Campus in Dhaka. The location of the site is presented in Fig. 1.

3 Equipment and materials for experimental study

3.1 Equipment used for testing

3.1.1 Shaking table

A shaking table facility is used for the experiment, as shown in Fig. 2. The base used for the test is made of steel. The length of the model is 2 m and has a width of 2 m. The shake table has a payload capacity of 1500 kg. The tablet can operate in a wide acceleration and frequency range, which varies from 0.05 g to 2 g and 0.05 Hz to 50 Hz, respectively. Also, the maximum displacement along the axis of motion has a range of ±200 mm. The machine was operated at a velocity of 30 cm/s.

3.1.2 Laminar box

A laminar box is used as the container for this experiment, which was designed with several considerations; maintain a small cross-section, water tightness of the model, very low resistance to soil settlement, and with a minimum shear stiffness and little mass. The box works as a large shear box with 24 hollow aluminum layers, as shown in Fig. 2. The container is designed in a way that the saturated granular soil can deform freely when subjected to a seismic motion. The container has several components, the base plate and the saturation and drainage system in the floor, the upper and the side guides, layers, and ball bearings, and an elastic internal membrane. The upper and side guides prevent the frame from any kind of deformation and hold it strongly. The diameter of the ball bearings is 12 mm. The ball bearings are placed in a hemispherical space to reduce the friction working as a column, also reducing the risk of deformation of the surface.

Each layer has an inward frame, with a dimension of 915 mm × 1220 mm × 1220 mm. The distance between any two consecutive layers is 2 mm. Also, to reduce the boundary effect, an embankment is constructed with soft clayey soil. The base layer is attached strongly with the base plate, which has an equal base dimension to the inner frame, only the height is 15 mm. Detailed setup and procedure are described in Hore *et al*. (2021).

3.1.3 Membrane and portable pluviator

A rubber membrane is placed inside the laminar box. Its thickness is 2 mm and the purpose is to use it to provide airtightness. It also prevents the soil from meeting walls or bearings directly. A portable pluviator, developed by Hossain and Ansary (2018), is used in the test.

3.2 Materials used in the experimental model

3.2.1 Dhaka clay soil

In this experiment, the prototype soil targeted is Dhaka soil. The samples are stiff, reddish-brown with homogeneous samples. At first, they were dried in an oven. Then, a wooden hammer was used to powder the dry lumps of soil. The sample was then sieved through a #200 standard sieve to obtain clean clay dust. The specific gravity of the soil was found to be 2.64, as determined by a lab test. The results also determined the value of the mean value liquid limit and plastic limit (PL), as shown in Table 1. The value of the plastic limit is located below the A-line, elucidated by the relation PI = 0.73(LL-20). As per the unified soil classification system (USCS), the soil is found to be lean clay (CL). Figure 3 shows the soil classification chart by USCS.

Reconstituted clay soil

Burland (1990) illustrated that shear strength and compressibility of clay soil in both the consolidated and over consolidated state delivers a source to understand the conforming properties of the in-situ natural clay soil. Hence, using the method stated by Burland (1990), Dhaka clay is reconstructed by carefully composing the oven-dried clay powder. Here, the initial water content is equal to the liquid limit (LL). A 'Hobart' rotary mixer is used to thoroughly mix the slurry. Then in the laminar

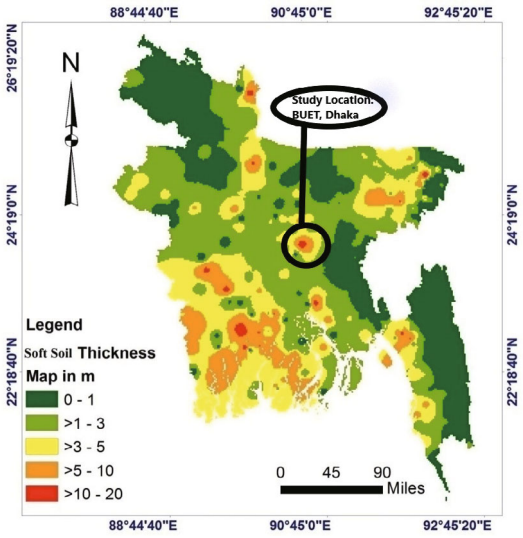

Fig. 1 Zonation of soft soil in Bangladesh (Hore *et al*., 2019)

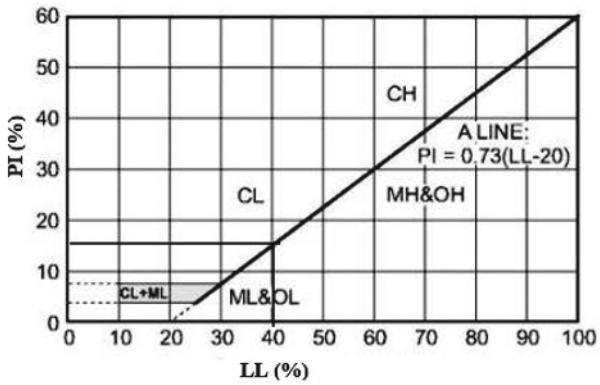

Fig. 2 Soil classification chart (USGS)

box, a 300 mm thick conformed clay is developed. The detailed procedure for the construction of reconstituted of clay soil is described in Chakraborty *et al*. (2021b). A settlement vs time graph is plotted by monitoring the consolidation process, and thereby mechanical dial gauges were calibrated and placed on the side of the box. The placement of clay soil and conduction of unconsolidated undrained (UU) test. The isotropic condition at loads with sensor arrangement. The curve provides insight into the gradual collapse of the soil structure, showing the weakening of the bond among the soil particles. The settlement increases once the dissipation becomes more rapid. However, in this process, pore water pressure reduces. The preparation of base clay soil is shown in Fig. 4. The loading pattern is shown in Fig. 5. Figure 6 shows the sensor arrangement with the average settlement curve.

In the case of saturated clay, the UU triaxial test is favorable for facilitating the exact field condition. UU triaxial tests are performed for all tests. The shear rate is 1.5 mm/min, and the applied confining stresses are 50 kPa and 100 kPa for reconstituted soil samples. The value of the applied confine stresses are 50 kPa and 100 kPa for the reconstituted clayey soil samples. The undrained strength (S_u) value is found to be 28 kPa.

3.2.2 Wrap faced embankment (sandy soil) with reinforcement

For backfill material, locally Sylhet sand is used in this study for the availability of the sand. The two types of sand, called Sylhet sand and local sand, are locally available. The particle size distribution curve is detailed in Fig. 7. According to USCS, the sand is defined as

Table 1 Clay soil parameters

Parameter	Clay soil	Unit
Unit weight (γ)	15	kN/m^3
Initial void ratio (e_o)	0.71	-
Specific gravity	2.64	-
Liquid limit (LL)	41	%
Plastic limit (PL)	16	%
Cohesion (c)	28.0	kN/m^2

Fig. 3 Shaking table test apparatus

Fig. 4 Preparation of clay soil

Fig. 5 Loading arrangement

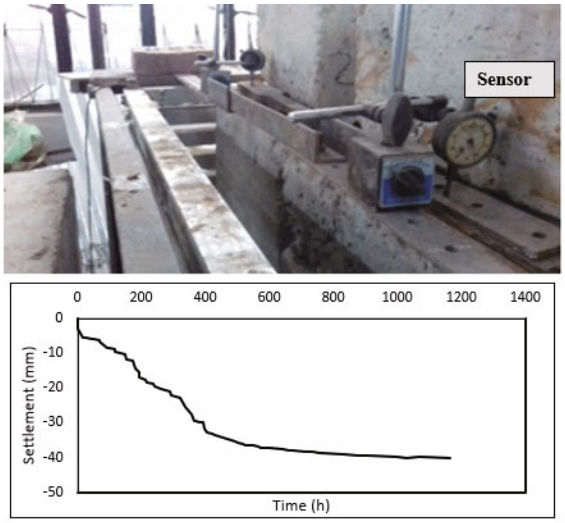

Fig. 6 Sensor arrangement with settlement curve

poorly graded sand (SP). The general geotechnical characteristics of the sands are shown in Table 2. To reinforce the sand in the test, a woven polypropylene multifilament geotextile (D50) is used (Hore *et al*., 2021). This individual multifilament is developed in such a way that it ensures the stability of each of the dimensions.

3.3 Model construction and testing protocol

3.3.1 Height of clay layer

The tests are demonstrated with clayey soil. The height is 300 mm, and a 50 mm sand blanket is placed above as shown in Fig. 8. Geotextile with an area of 1 m^2 was placed between these two layers. The toe of the wall may have a proclivity towards free sliding. The height of the prototype wall is 3 m, with a scale factor of 1/10. The cone penetration test was executed to measure and quantify the characteristics of the total clayey soil layer after the development.

3.3.2 Preparation of wrap faced embankment

The portable pluviator is used for the preparation of the wrap faced embankment. The relative density was maintained at 48% for the sands. Four layers are constructed to prepare the embankment. Figure 9 shows the preparation of wrap faced embankment.

3.3.3 Sensor arrangement and surcharge load

To measure the acceleration, displacement, shear strain, and pore water pressure, four different types of sensors are deployed in the model. For monitoring and measuring the accelerations of the developed model along with a vertical array, accelerometers are used. To monitor the displacement of the sand model wall along the horizontal direction, LVDT transducers are deployed. Four strain gauges are attached to the geotextile to measure the shear strain response. The two

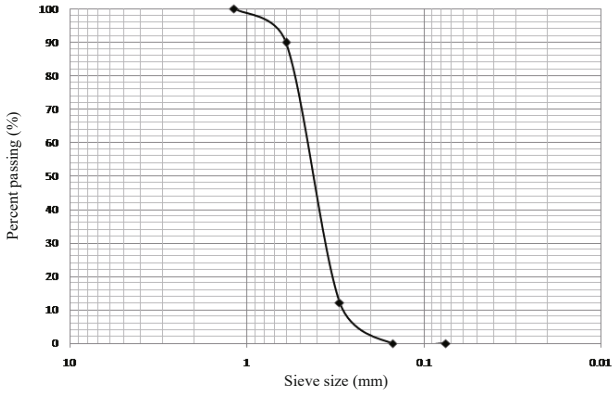

Fig. 7 Particle size distribution curve of the sand

Table 2 Properties of sand

Physical properties	Properties of sand
Coefficient of uniformity, C_u	2.00
Coefficient of curvature, C_c	0.96
Effective size, D_{10} (mm)	0.40
Average size, D_{50} (mm)	0.72
Specific gravity, G_s	2.66
Friction angle (°)	31
Void ratio	0.53
Fineness modulus, *FM*	2.63
Maximum dry density (kN/m^3)	16.40
Minimum dry density (kN/m^3)	13.50
Relative density, *D*r (%)	48
USCS soil classification	Poorly graded sand (SP)

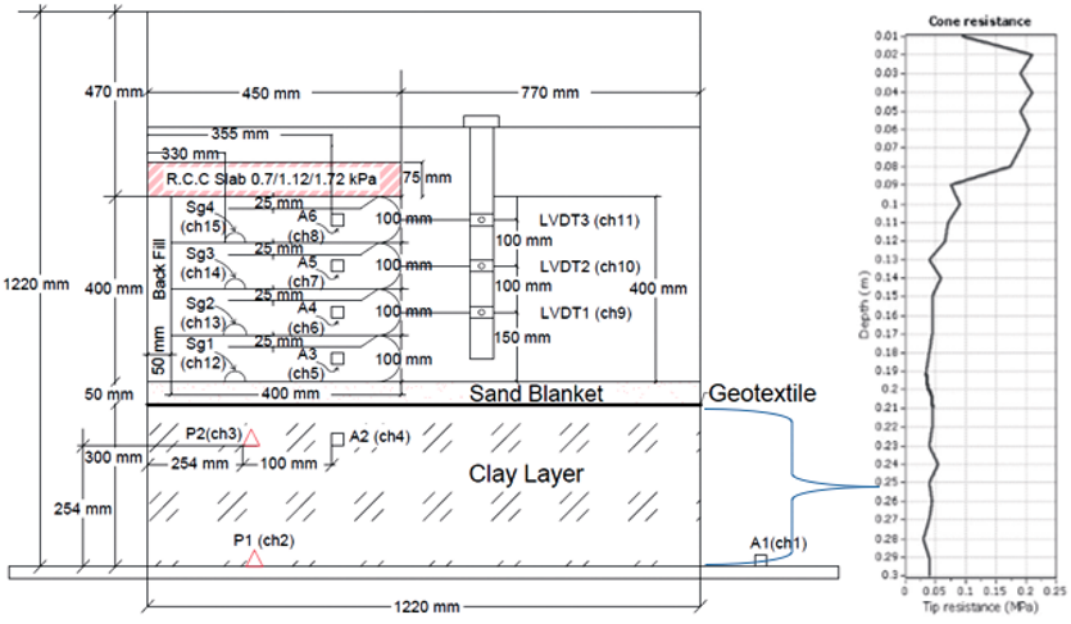

Fig. 8 Experimental setup

sensors that measure pore-water pressure are placed in the clay soil layer. In total, fifteen data channels are used; the arrangements of the different sensors are shown in Fig. 10. The fifteen sensors in this research are very significant for measuring the different soil parameters. Proper placement is important to ensure accurate results of the research. For this demonstration, three different surcharge loads are used. The loads are 0.7 kPa, 1.12 kPa, and 1.72 kPa.

3.3.4 Prototype-model similitude

Due to the boundary conditions, and the stress-dependent behavior of the soil, precise modeling is essential. The model size is scaled according to the facility available for the test. The soil walls and reinforcement properties were precisely maintained, and as per requirements, 1-g shaking tests were performed. This ensured the accuracy of the behavior prediction of the prototype structure. The prototype modelling is the base on the soil conditions, geographical location and pattern of the structure. Achieving similitude with the prototype wall is not always ensured even if the scale is correct. In low-stress limits, 1-g shake table tests cannot predict the exact results of the prototype, but when it comes to the reinforced model wall, the prediction becomes much more accurate (Hore *et al*., 2021). The scaling factor is given in Table 3.

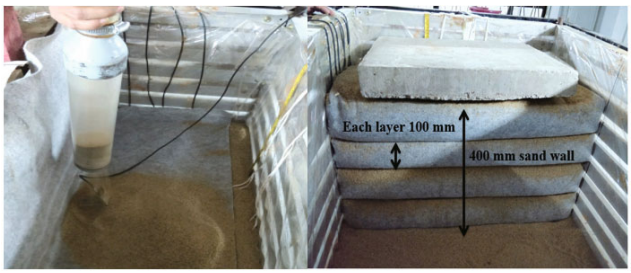

Fig. 9 Preparation of wrap-faced wall

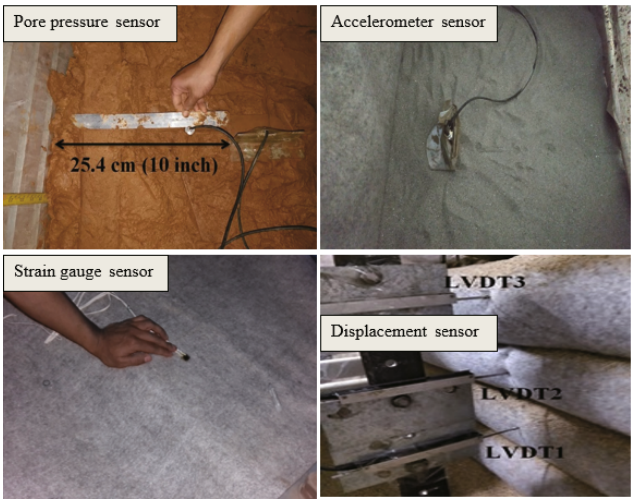

Fig. 10 Different sensor arrangements

3.3.5 Input motions

Earlier literature by Sabermahani *et al*. (2009) and Chakraborty *et al*. (2021) showed that the harmonic sinusoidal base acceleration has more strength and can cause more damage than an archetypical earthquake with the same fundamental frequency and amplitude. Matsuo *et al*. (1998) analyzed the theory in the published literature. To avoid resonance, the applied frequency should vary widely from the fundamental frequency of the wall, and the different input motions based on the acceleration, amplitude and surchrage of the different test patterns should be used. In this research, the Kobe earthquake with different input accelerations of 0.05 g, 0.1 g, 0.15 g, and 0.2 g are used. Table 4 shows the sequence of the experimental tests.

3.4 PLAXIS 3D model

In this research, PLAXIS 3D is used as a numerical method for the analysis of the model. PLAXIS is a finite element package and was industrialized for the investigation of displacement, stability, and flow in geotechnical engineering projects. The PLAXIS 3D software (Brinkgreve and Broere, 2006) uses quadratic tetrahedral 10-node elements. In this research, the numerical analysis is performed on the wrap faced embankment based on the different accelerations of earthquake response. The sequences for the steps of modeling are model geometry and boundary condition, soil properties, structural model, mesh generation and dynamic properties, and analysis and output results. The boundary condition of the model are shown in Table 5.

3.4.1 Soil stratigraphy and structural element

A borehole is defined in the soil layers. The soil layers comprise the embankment foundation, and the wrap embankment layers are also defined. This is done in the Structures mode. The coordinate of the borehole is at (0 0 0). Soil material data sets are created according to Table 6. The soil materials data sets are assigned to the corresponding layers in the borehole. The different soil parameters and structural element are input on the

Table 3 Scaling factors for experimental test (Kokusho, 1980; Yu and Richart, 1984)

Parameters	Symbol	Scale factor	Scale factor Prototype/Model
Acceleration	a	1	1
Length	L	1/N	10
Strain	ε	$1/N^{1-\alpha}$	3.125
Stiffness	G	$1/N^{\alpha}$	3.125
Displacement	d	$1/N^{2-\alpha}$	32.25
Frequency	f	$N^{1-\alpha/2}$	0.18
Force	F	$1/N^{3}$	1000
Force/Length	F/L	$1/N^{2}$	100
Time	t	$1/N^{1-\alpha/2}$	5.62

interface of the numerical model. The experimental input parameters are used in the PLAXIS 3D model. The details of the segment′s characteristics are shown in Fig. 11. The extrude object button was the click. The creation of the whole structure is shown in Fig. 12.

3.4.2 Dynamic properties, mesh generation, and output results

Dynamic loads are defined based on input values of loads. This is also defined by prescribed displacements and corresponding time-dependent multipliers, such as the amplitude, phase, and frequency. The Kobe earthquake is defined as shown in Fig. 13. The output results are found from the software interface and the analysis of the calculated values. The output result of three parameters: deformation response, excess pore water pressure response, and strain response are presented in Figs. 14 to 16.

4 Results and discussions

The dynamic properties of soil, for instance acceleration amplification, displacement, excess pore water pressure, and percentage of strain, are presented in this section. The effect of acceleration and different types of surcharges are also analyzed. The response data are presented for the tests KST1, KST2, KST3, KST4, KST5, and KST9 using Kobe earthquake loading. All responses are measured against two parameters, the effect of input base acceleration and the effect of surcharge loading. KST1, KST2, KST3, and KST4 are taken for analysis to account for the effects of acceleration amplification, and KST1, KST5, and KS9 are taken for analysis to measure the effects of the surcharge load effect. Also, input acceleration values of 0.05 g, 0.10 g, 0.15 g, and 0.20 g are used as the measurement.

Table 4 Test sequence for model

Name of tests	Base acceleration a_{max} (g)	Relative density R_d (%)	Surcharge (kPa)
KST1	0.05	48	1.72
KST2	0.10	48	1.72
KST3	0.15	48	1.72
KST4	0.20	48	1.72
KST5	0.05	48	1.12
KST9	0.05	48	0.70

4.1 Response of acceleration

Acceleration amplification for earthquake excitation has a significant role to measure the acceleration response of different elevations. The elevation of the model is noted as z and full height as T. At the top of the wall, the acceleration amplification is maximum for all the tests. The time acceleration histories (KST1) are

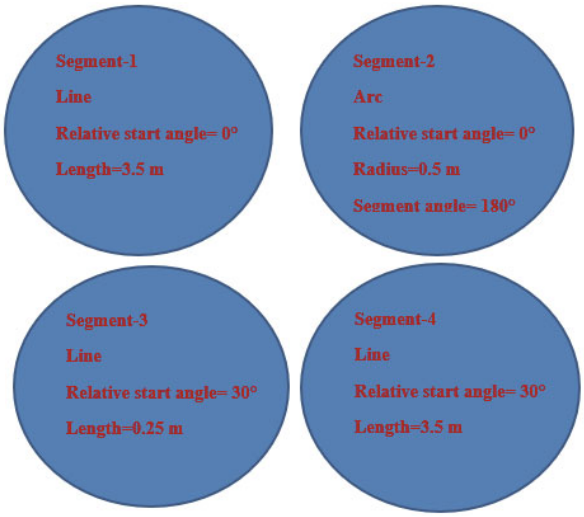

Fig. 11 Poly curve with segment type in PLAXIS

Table 5 Model boundary conditions

Layer	Boundary limits	X_{min}	X_{max}	Y_{min}	Y_{max}	Z_{min}	Z_{max}
Clay	X=0 to 2.6 m Y=0 to 0.2 m Z=-0.35 to -0.05 m	Free	Free	Fixed	Fixed	Fixed	Free
Sand	X=0 to 2.6 m Y=0 to 0.2 m Z=-0.05 m to 0	Free	Free	Fixed	Fixed	Free	Free
Bottom (wrap faced)	X=0 to 0.45 m Y=0 to 0.2 m Z=0 to 0.1 m	Free	Free	Fixed	Fixed	Free	Free
Middle 1 (wrap faced)	X=0 to 0.45 m Y=0 to 0.2 m Z=0.1 to 0.2 m	Free	Free	Fixed	Fixed	Free	Free
Top (wrap faced)	X=0 to 0.45 m Y=0 to 0.2 m Z=0.3 to 0.4 m	Free	Free	Fixed	Fixed	Free	Free

shown in Fig. 17. This observation was in consensus with the results of physical tests reported by Murata *et al*. (1994) and El-Emam and Bathurst (2007) and Krishna and Bhattacharjee (2019).

4.1.1 Effect of input acceleration

The acceleration amplifications along the elevation of the wall are found from different shake table tests (KST1, KST2, KST3, and KST4) and different PLAXIS 3D models (KST1(P), KST2 (P), KST3(P), and KST4(P)). The different base accelerations are 0.05 g, 0.10 g, 0.15 g, and 0.2 g. In this case, the surcharge pressure and relative density are 1.72 kPa and 48%, respectively, and are presented in Fig. 18. The acceleration amplification increased with the increase of base acceleration at all elevations, as depicted in the figure. The maximum acceleration amplification is 1.59 from the shake table results and 1.70 from the PLAXIS 3D model as seen in Table 7. The acceleration amplification decreased to 1.29 from the shake table test results and 1.39 from the PLAXIS 3D model at the acceleration of 0.05 g. Acceleration amplification is higher at the peak height, and the overburden pressure is lower compared to the bottom of the wall. The overburden pressure was lower at the top of the wall and significantly higher at the bottom of the wall. Due to higher overburden pressure at the bottom of the wall, the acceleration amplification is decreased at the bottom layer. From the same figure, it can also be observed that the present study is linked with the study of Krishna and Latha (2007). The pattern of amplification for the current study and the study of Krishna and Latha (2007) are almost same where T4, T6 and T7 model tests for 0.1 g, 0.15 g and 0.2 g. Acceleration amplifications increased with base accelerations in all cases. The variation of PLAXIS 3D output results from the shake table model test is 6.92% and 7.75% higher, respectively, than for maximum and minimum acceleration amplifications.

4.1.2 Effect of surcharge

The KST1, KST5, and KST9 for experimental and KST1(P), KST5(P), and KST9(P) for numerical are

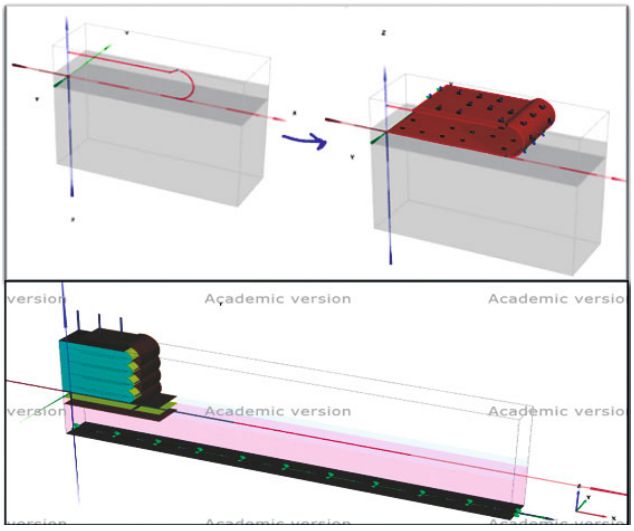

Fig. 12 Creation of whole structure in PLAXIS

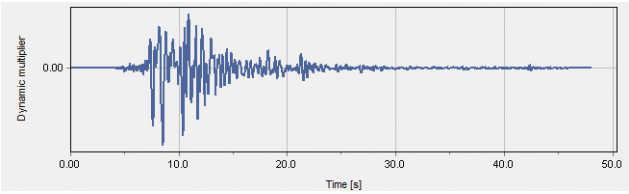

Fig. 13 Kobe earthquake

Table 6 Subsoil and embankment soil properties

Input parameter	Symbol	Sylhet sand	Clay
Material model	Model	Hardening soil	Soft soil
Drainage type	Type	Drained	Under. (A)
Unit weight of soil (kN/m^3)	γ_{unsat}	15	14.8
Initial void ratio	e_o	0.63	0.69
Secant stiffness in standard drained (kN/m^2)	E_{50}^{ref}	25.0×10^3	-
Tangent stiffness for primary oedometer loading (kN/m^2)	E_{oed}^{ref}	25.0×10^3	-
Unloading / reloading stiffness (kN/m^2)	E_{ur}^{ref}	75.0×10^3	-
Modified compression index	λ	-	0.17
Modified swelling index	K	-	0.04
Cohesion (kN/m^2)	C	2.0	29.0
Friction angle	Φ	31	1.0
Horizontal permeability (x-direction) (m/day)	k_x	24.89	0.06
Horizontal permeability (y-direction) (m/day)	k_y	24.89	0.06
Vertical permeability (m/day)	K_z	24.89	0.06

depicted in Fig. 19. The response of acceleration against different surcharge pressures is also described in this figure. The surcharge pressures are 1.72 kPa, 1.12 kPa, and 0.7 kPa at the fixed base acceleration (0.05 g). The maximum acceleration amplification is 1.67 from the shake table results and 1.69 kPa from the PLAXIS 3D model at a surcharge of 0.7 kPa. The acceleration amplification decreased to 1.31 from the shake table results and 1.41 kPa from the PLAXIS 3D model at a surcharge of 1.72 kPa as seen in Table 7. The acceleration amplification at all elevations decreased with surcharge load, which also can be seen from Fig. 19. The result of an increase in the surcharge pressure causes an increase in overburden pressure. As a result, the soil becomes less amplified. A contrast of the present study with the study of Krishna and Latha (2007) is depicted in Fig. 18. In the figure, the model tests T4, T6 and T7 is the test for the 0.1 g, 0.15 g and 0.20 g of the Lata′s test. The variation of results from PLAXIS 3D analysis for acceleration amplification (maximum and minimum values) is 1.20% and 7.63% higher than the results from the shake table respectively.

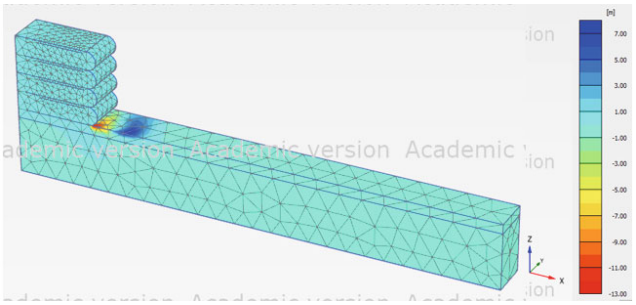

Fig. 14 Displacement response

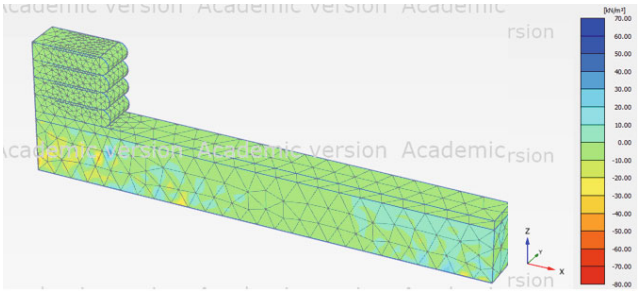

Fig. 15 Excess pore water pressure response

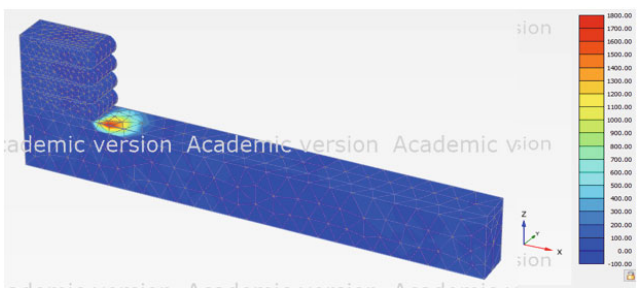

Fig. 16 Strain response

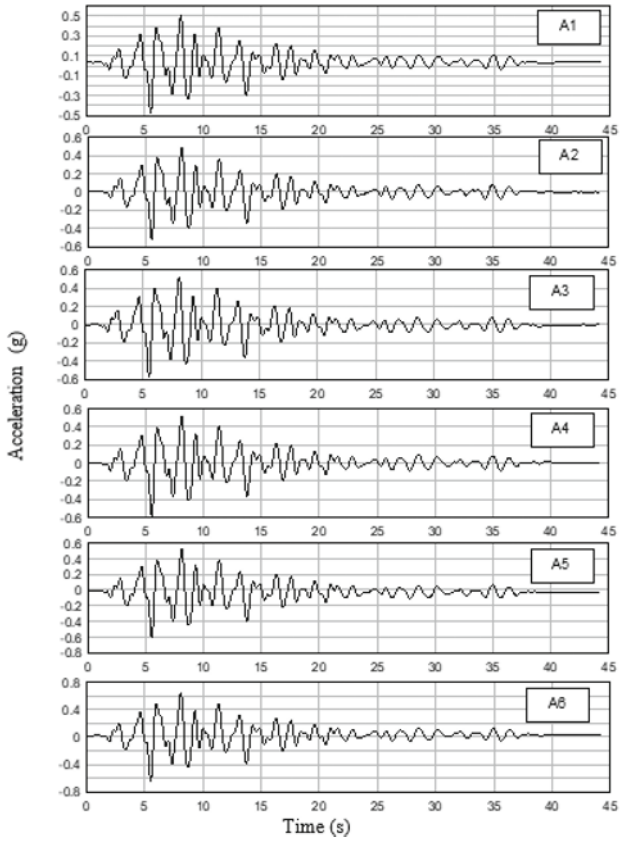

Fig. 17 Time acceleration histories (KST1)

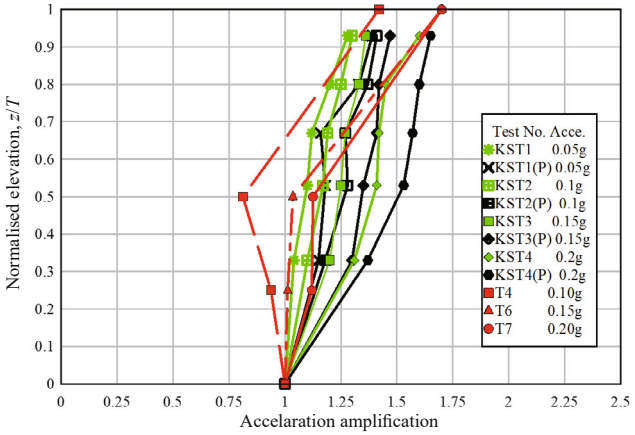

Fig. 18 Effect of base acceleration on acceleration amplification (KST1-KST4)

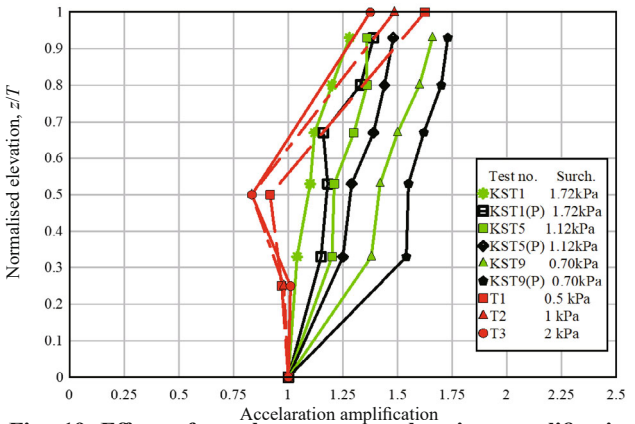

Fig. 19 Effect of surcharge on acceleration amplification (KST1, 5, and 9)

Table 7 Acceleration amplification responses

Test name	Parameters	Layer of sand location	Shake table results	PLAXIS 3D results	Variation of results (%)
KST1	Acceleration	A3	1.09	1.21	11.01
		A6	1.39	1.41	1.44
KST2		A3	1.21	1.31	8.26
		A6	1.29	1.39	7.75
KST3		A3	1.24	1.40	12.90
		A6	1.41	1.51	7.09
KST4		A3	1.47	1.49	1.36
		A6	1.59	1.70	6.92
KST1	Surcharge	A3	1.11	1.21	9.01
		A6	1.31	1.41	7.63
KST5		A3	1.19	1.32	10.92
		A6	1.35	1.51	11.85
KST9		A3	1.39	1.59	14.39
		A6	1.67	1.69	1.20

4.2 Displacement response

Three linear vertical displacement transducers (LVDTs) were used to measure the horizontal displacement of the wrap-faced embankment as shown in Fig. 8. The time displacement histories for Kobe earthquake excitation are presented in Fig. 20. Here, the total height of the embankment is noted as H and elevation and horizontal displacement as z and δh, respectively. The observation of the research is in agreement with the tests performed by Krishna and Latha (2007) and Krishna and Bhattacharjee (2019).

4.2.1 Effect of input acceleration

Figure 21 depicts the combination of acceleration from tests KST1, KST2, KST3 and KST4 for experimental and KST1(P), KST2(P), KST3(P), and KST4(P) for numerical analysis, respectively. At a standardized elevation of z/H=0.875, the standardized displacements are relatively high at higher base accelerations. The maximum horizontal displacement of 1.27% of the total wall height (H), from the shake table, results in 0.20 g. The observed displacement is compared with 0.35% for 0.05 g base accelerations. The maximum displacement is 0.510 mm at an acceleration of 0.2 g from shake table results and 0.540 mm from the PLAXIS 3D model. The displacement decreased to 0.140 mm from the shake table results and 0.153 mm from the PLAXIS 3D model at an acceleration of 0.05 g as shown in Table 8. This phenomenon had similarities to the test results of Sakaguchi *et al*. (1992) and Krishna and Latha (2007). Displacement is higher and the overburden pressure is lower at peak height when compared with the values at the bottom of the wall. The overburden pressure is higher at the bottom of the layer due to surcharge plus four layers of the wrap faced embankment. On the other hand, the difference between the numerical and experimental result is significant. The variation from PLAXIS 3D results (maximum and minimum displacements) is 2.20% and 7.19% higher than the results from shake table tests.

4.2.2 Effect of surcharge

The standardized displacement profile is found from tests KST1, KST5 and KST9 for the experimental model and KST1(P), KST5(P), and KST9(P) for the numerical model. The base acceleration (0.05 g) provided an understanding of the effect of different surcharge loadings as shown in Fig. 22. The inversely proportional at all elevations is found in the test parameters. The maximum displacement of the wall is ($\delta h/H$=1.03%) from the shake table results in a surcharge pressure of 0.7 kPa. The displacement decreased to ($\delta h/H$=0.35%)

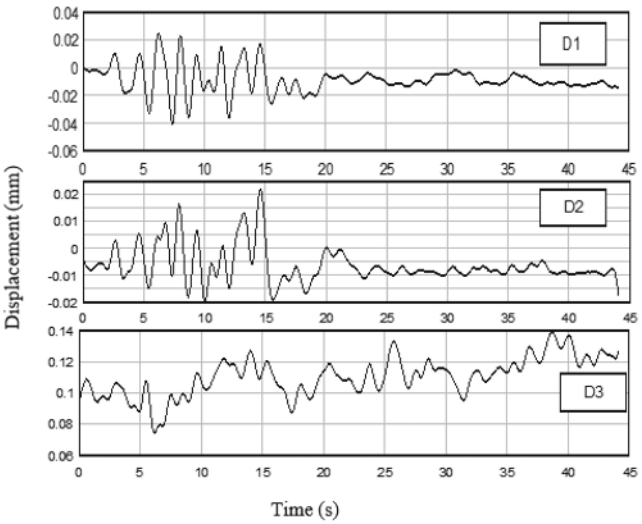

Fig. 20 Time displacement histories (KST1)

at a surcharge pressure of 1.72 kPa. The maximum displacement is 0.410 mm from the shake table results and 0.440 mm from the PLAXIS 3D model at a surcharge of 0.7 kPa. The displacement decreased to 0.140 mm from shake table results and 0.153 mm from the PLAXIS 3D model at a surcharge of 1.72 kPa as shown in Table 8. Moreover, the test results and findings are the same when compared with Krishna and Latha (2007). The variation from PLAXIS 3D results (maximum and minimum displacements) is 7.09% and 7.97% higher than the results from the shake table tests.

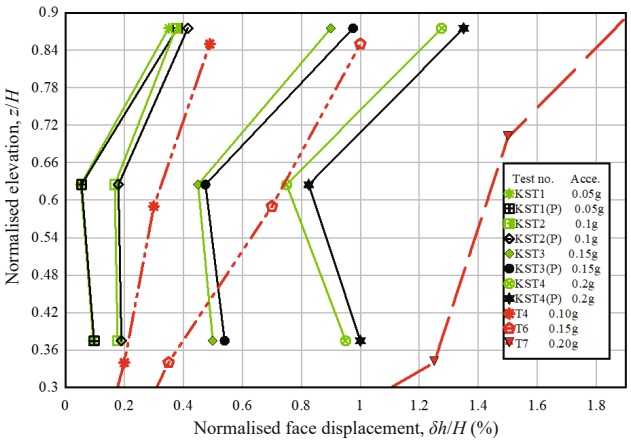

Fig. 21 Effect of base acceleration on displacement profile (KST1-KST4)

4.3 Excess pore water pressure response

Time and excess pore water pressure histories are presented in Fig. 23. Here, note that the height of the clay layer (S) of the embankment is 300 mm. The two-pore water pressure sensors are used to measure the excess pore water pressure of the clay foundation of different elevations. The effect of input acceleration and surcharge are described in this section.

4.3.1 Effect of input acceleration

The excess pore water pressure along the height of the clay layer is found from tests KST1, KST2, KST3, and KST4 for the experimental model and KST1(P),

Table 8 Displacement responses

Test name	Parameters	Layer of sand location	Shake table results (mm)	PLAXIS 3D results (mm)	Variation of results (%)
KST1	Acceleration	2nd layer (2nd bottom)	0.041	0.044	7.32
		3rd layer (mid)	0.018	0.019	5.56
		4th layer (top)	0.139	0.149	7.19
KST2		2nd layer (2nd bottom)	0.069	0.076	10.14
		3rd layer (mid)	0.071	0.080	12.68
		4th layer (top)	0.141	0.155	9.93
KST3		2nd layer (2nd bottom)	0.211	0.221	4.74
		3rd layer (mid)	0.179	0.188	5.03
		4th layer (top)	0.359	0.391	8.91
KST4		2nd layer (2nd bottom)	0.379	0.411	8.44
		3rd layer (mid)	0.311	0.333	7.07
		4th layer (top)	0.499	0.510	2.20
KST1	Surcharge	2nd layer (2nd bottom)	0.041	0.043	4.88
		3rd layer (mid)	0.022	0.023	4.55
		4th layer (top)	0.138	0.149	7.97
KST5		2nd layer (2nd bottom)	0.147	0.159	8.16
		3rd layer (mid)	0.211	0.229	8.53
		4th layer (top)	0.248	0.279	12.50
KST9		2nd layer (2nd bottom)	0.211	0.221	4.74
		3rd layer (mid)	0.309	0.341	10.36
		4th layer (top)	0.409	0.438	7.09

KST2(P), KST3(P), and KST4(P) for numerical model, and is shown in Fig. 24. The base accelerations are 0.05 g, 0.10 g, 0.15 g, and 0.20 g for the surcharge load of 1.72 kPa. The directly proportional phenomenon is shown for the excess pore water pressure response against base acceleration variation. The pore water pressure is 0.941 kPa from the shake table results and 1.039 kPa from the PLAXIS 3D model at an acceleration of 0.2 g. The excess pore water pressure decreased to 0.084 kPa from shake table results and 0.091 kPa from the PLAXIS 3D model at an acceleration of 0.05 g as shown in Table 9. The variation of results from PLAXIS 3D is 10.41% and 8.33% higher than the results from the shake table tests.

4.3.2 Effect of surcharge

The tests KST1, KST5 and KST9 for the experimental model and KST1(P), KST5(P), and KST9(P) for the numerical results are conducted to find the excess pore water pressure and are presented in Fig. 25. The surcharge pressure is 1.72 kPa, 1.12 kPa, and 0.7 kPa for the base acceleration of 0.05 g. The maximum pore water pressure of the model is 0.079 kPa, 0.149 kPa, and 0.311 kPa, respectively. The maximum pore water pressure is 0.311 kPa from the shake table results and 0.321 kPa from the PLAXIS 3D model at a surcharge of 0.7 kPa. The excess pore water pressure decreased to 0.079 kPa from the shake table results and 0.089 kPa from the PLAXIS 3D model at a surcharge of 1.72 kPa as shown in Table 9. It is observed that pore water pressure response against surcharge variation was inversely proportional at all elevations of the clay foundation. When surcharge pressure increases, the pore water dissipates. Therefore, the pore pressure decreased due to a large surcharge. The variation of results from PLAXIS 3D is 3.22% and 12.66% higher than the results from the shake table tests.

4.4 Strain response

The time strain history profiles of earthquake excitations are presented in Fig. 26. The effect of input acceleration and surcharge response on the percentage of strain is presented in this section.

4.4.1 Effect of input acceleration

Figure 27 depicts the strain (%) profile from tests KST1, KST2, KST3, and KST4 for the experimental model and KST1(P), KST2(P), KST3(P), and KST4(P) for the numerical model. The base accelerations are 0.05 g, 0.10 g, 0.15 g, and 0.20 g. The maximum strain (%) is 3.28 from shake table results and 3.61 from the PLAXIS 3D model for 0.20 g. The strain (%) is 2.79 from shake table results and 3.05 from PLAXIS 3D model for 0.05 g base accelerations and can be seen in Table 10. The strain is more at the peak height. The findings on the values of strain obtained in the present study are consistent with the results presented by Wang *et al*. (2015). The variation of results from PLAXIS 3D are 10.06% and 9.32% higher than the results obtained from shake table tests.

4.4.2 Effect of surcharge

The strain (%) profiles are conducted for tests KST1, KST5 and KST9 for the experimental model and KST1(P), KST5(P), and KST9(P) for the numerical

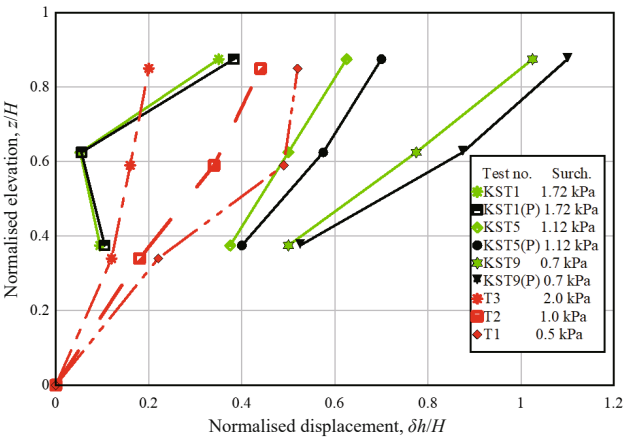

Fig. 22 Effect of surcharge on displacement profile (KST1, 5, and 9)

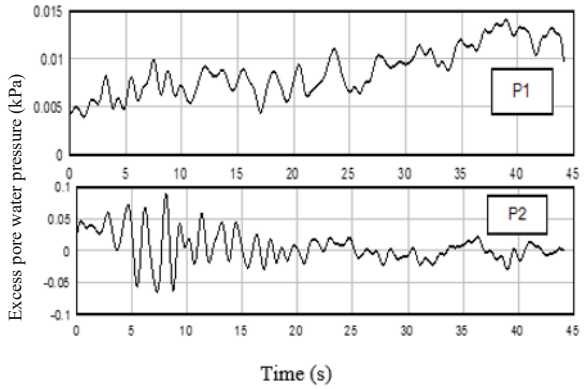

Fig. 23 Excess pore water pressure time histories (KST1)

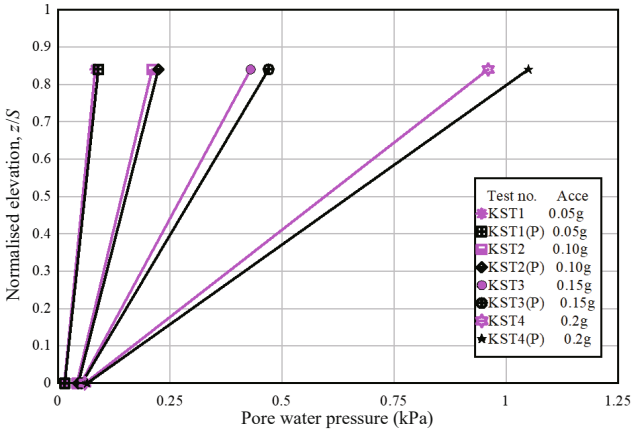

Fig. 24 Effect of base acceleration on pore water pressure (KST1-KST4)

model as shown in Fig. 28. It is observed that the strain (%) response against surcharge variation is inversely proportional at all elevations. The maximum strain (%) of the wall is 3.39 from the shake table results and 3.69 from the PLAXIS 3D model at a surcharge pressure of 0.7 kPa. The percentage of strain is decreased to 2.71 at a surcharge pressure of 1.72 kPa. The maximum strain (%) is 3.39 at a surcharge of 0.7 kPa, whereas it decreased to 2.74 from shake table results and 3.12 from the PLAXIS 3D model at a surcharge of 1.72 kPa as can be seen in Table 10. The variation of results from PLAXIS 3D is 8.85% and 13.87% higher than the results obtained from the shake table tests, respectively.

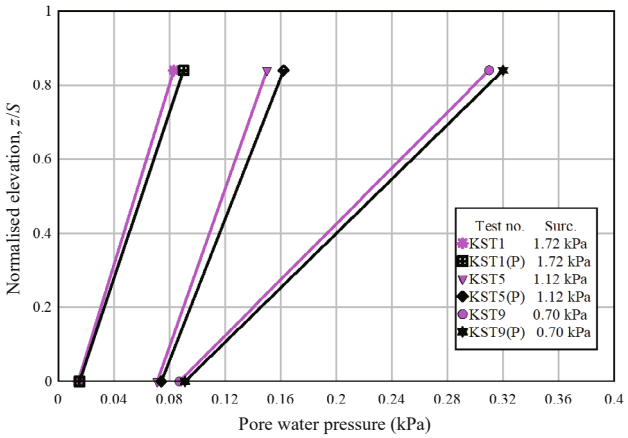

Fig. 25 Effect of surcharge on pore water pressure (KST1, 5, and 9)

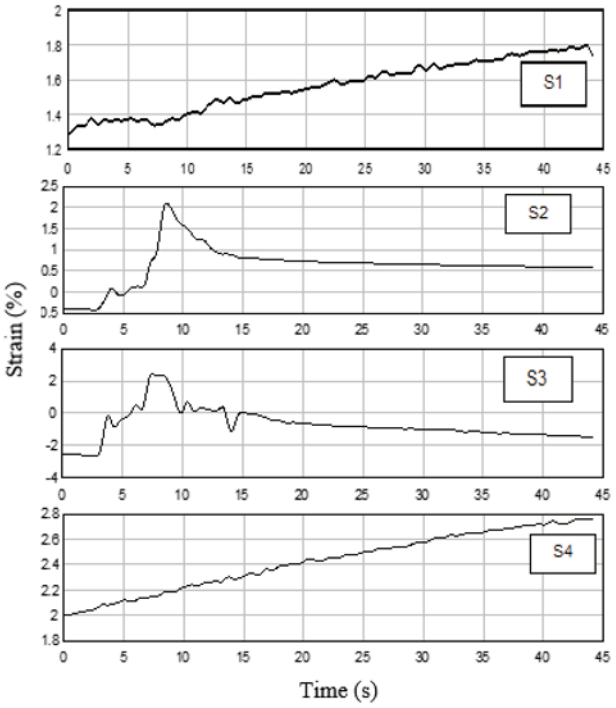

Fig. 26 Time strain histories (KST1)

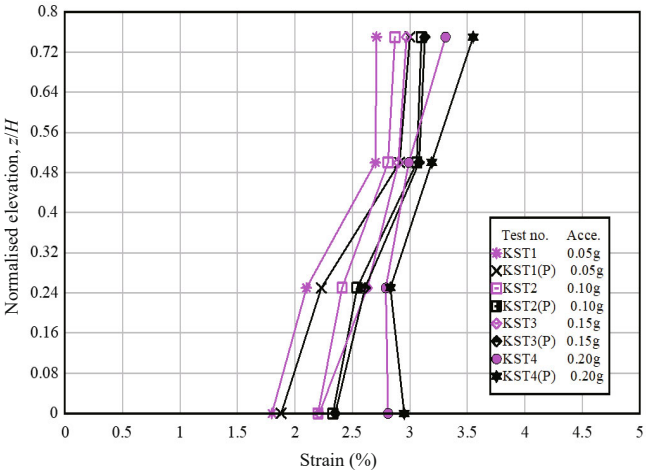

Fig. 27 Effect of base acceleration on strain (KST1-KST4)

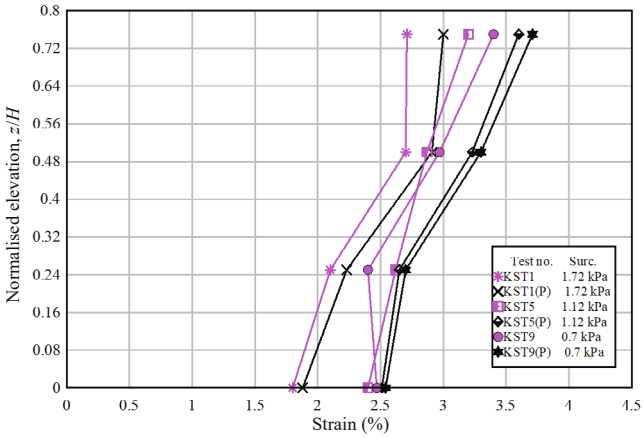

Fig. 28 Effect of surcharge on strain (KST1, 5 and 9)

Table 9 Excess pore water pressure responses

Test name	Parameters	Layer of sand location	Shake table results (kPa)	PLAXIS 3D results (kPa)	Variation of results (%)
KST1	Acceleration	P2 Location	0.084	0.091	8.33
KST2		P2 Location	0.211	0.235	11.37
KST3		P2 Location	0.431	0.471	9.28
KST4		P2 Location	0.941	1.039	10.41
KST1	Surcharge	P2 Location	0.079	0.089	12.66
KST5		P2 Location	0.149	0.159	6.71
KST9		P2 Location	0.311	0.321	3.22

Table 10 Strain responses

Test name	Parameters	Layer of sand location	Shake table results (%)	PLAXIS 3D results (%)	Variation of results (%)
KST1	Acceleration	Sg1 (Bottom)	1.76	1.89	7.39
		Sg4 (Top)	2.81	3.12	11.03
KST2		Sg1 (Bottom)	2.19	2.41	10.05
		Sg4 (Top)	2.79	3.05	9.32
KST3		Sg1 (Bottom)	2.31	2.40	3.90
		Sg4 (Top)	2.89	3.09	6.92
KST4		Sg1 (Bottom)	2.79	2.88	3.23
		Sg4 (Top)	3.28	3.61	10.06
KST1	Surcharge	Sg1 (Bottom)	1.78	1.91	7.30
		Sg4 (Top)	2.74	3.12	13.87
KST5		Sg1 (Bottom)	2.39	2.48	3.77
		Sg4 (Top)	3.18	3.51	10.38
KST9		Sg1 (Bottom)	2.51	2.57	2.39
		Sg4 (Top)	3.39	3.69	8.85

5 Summary and conclusions

Shake table experiments on a wrap faced geotextile model wall were performed under nine different dynamic motions with four base accelerations and three different surcharge loads using a fixed relative density of the Kobe earthquake. Finite element analysis (FEA) using PLAXIS 3D software was used to analyze and compare the numerical prediction with the experimental results. The results from the PLAXIS 3D analysis were slightly higher than the experimental results. There were minor differences in results between the numerical analysis and the experimental study, which were numerically less than 15%. However, the evaluation of the results extracted from the numerical analysis and the physical modeling showed good agreement, thus validating the authenticity of the numerical model. Both the results and the response of the embankment with soft clayey soil was significantly affected by the base acceleration levels and magnitude of surcharge pressure placed on the crest of the wrap faced soil wall. The results from the experimental and numerical analysis are summarized as follows.

- Acceleration amplifications values were higher when base accelerations were increased. Accelerations at the top of the wall were inversely proportional to the surcharge pressures from the tests.
- The standardized displacements were relatively high at higher base accelerations where the displacement response against surcharge variation was inversely proportional to all elevations.
- Porewater pressure was produced due to the entrapped water remaining within the Clay sample. The water has been added to the dry clay powder during the clay sample preparation. The water still remained after the one-dimensional consolidation process. The pore water pressure was comparatively higher within the clay mass and lower at the side edges.
- The strains at the bottom layer were minimal, and the strains of the top layer were the largest, indicating that the geotextiles placed at the uppermost layer improved the performance of the seismic stability.

The findings from this study will help to better predict the dynamic behavior of wrap-faced embankments and can be used to more accurately adjust the design parameters at the discretion of the engineer.

References

Bathurst RJ and Hatami K (1998), "Seismic Response Analysis of a Geosynthetic-Reinforced Soil Retaining Wall," *Geosynthetics International*, **5**(1–2): 127–166. https://doi.org/10.1680/gein.5.0117

Bhattacharjee A and Krishna AM (2013), "Development of Numerical Model of Wrap-Faced Walls Subjected to Seismic Excitation," *Geosynthetics International*, **19**(5): 354–369. doi:10.1680/gein.12.00022

Brinkgreve RBJ and Broere W (2006), *Plaxis 3D Foundation Version 1.5*, Plaxis B.V., Delft, Netherlands.

Burland JB (1990), "On the Compressibility and Shear Strength of Natural Clays," *Geo Technique*, **40**(3): 329–378.

Cengiz C and Guler E (2018), "Shaking Table Tests on Geosynthetic Encased Columns in Soft Clay," *Geotextiles and Geomembranes*, **46**(6): 748–758. https://doi.org/10.1016/j.geotexmem.2018.07.009

Chakraborty S, Hore R, Shuvon AM, Kamrul K and Ansary MA (2021a), "Physical and Numerical Analysis of Reinforced Soil Wall on Clayey Foundation Under

Repetitive Loading: Effect of Fineness Modulus of Backfill Material," *Arab J Geosci*, **14**: 1108. https://doi.org/10.1007/s12517-021-07317-7

Chakraborty S, Hore R, Shuvon AM, Mazhar MS and Ansary MA (2021b), "Dynamic Responses of Reinforced Soil Model Wall on Soft Clay Foundation," *Geotech Geol Eng*, **39**: 2883–2901. https://doi.org/10.1007/s10706-020-01665-z

Choudhury D, Nimbalkar SS and Mandal JN (2006), "Comparison of Pseudo-Static and Pseudo-Dynamic Methods for Seismic Earth Pressures on Retaining Wall," *J. Ind. Geophys Union*, **10**(4): 263–271.

Damians IP, Bathurst RJ, Olivella S (2021), "3D Modelling of Strip Reinforced MSE Walls," *Acta Geotech*, **16**: 711–730. https://doi.org/10.1007/s11440-020-01057-w

Edinçliler A and Güler E (1999), "Geotextile-Reinforced Embankments on Soft Clays-Effects of a Foundation Soil Crust Strengthened by Lime Diffusion," *Geosynthetics International*, **6**(2): 71–91.

El-Emam MM and Bathurst RJ (2007), "Influence of Reinforcement Parameters on the Seismic Response of Reduced-Scale Reinforced Soil Retaining Walls," *Geotextile Geomembrane*, **25**(1): 33–49.

Gidday BG and Mittal S (2020), "Improving the Characteristics of Dispersive Subgrade Soils Using Lime," *Heliyon*, **6**(2): e03384. https://doi.org/10.1016/j.heliyon.2020.e03384

Hore R, Arefin MR and Ansary MA (2019), "Development of Zonation Map Based on Soft Clay for Bangladesh," *Journal of Engineering Science*, **10**(1): 13–18.

Hore R, Chakraborty S and Ansary MA (2021), "Seismic Response of Embankment on Soft Clay Based on Shaking Table Test," *Int. J. of Geosynth. and Ground Eng*., **7**:3. https://doi.org/10.1007/s40891-020-00246-7

Hore R, Chakraborty S, Bari MF, Shuvon AM, Ansary MA (2020), "Soil Zonation and the Shaking Table Test of the Embankment on Clayey Soil, Geosfera Indonesia," **5**(2): 196–209. DOI: https://doi.org/10.19184/geosi.v5i2.17873

Hore R, Chakraborty S, Shuvon AM and Ansary MA (2022), "Numerical Verification for Seismic Response of Reinforce Soil Embankment on Soft Clay Foundation," *Geotechnical Engineering Journal of the SEAGS & AGSSEA*.

Hossain MZ and Ansary MA (2018), "Development of a Portable Traveling Pluviator Device and Its Performance to Prepare Uniform Sand Specimens," *Innovative Infrastructure Solutions*, **3**(1): 53.

Huang CC (2019), "Seismic Responses of Vertical-Faced Wrap-Around Reinforced Soil Walls," *Geosynthetics International*, **26**(2): 146–163. DOI: https://doi.org/10.1680/jgein.18.00044

Huang CC and Wang WC (2005), "Seismic Displacement of a Geosynthetic-Reinforced Wall in the 1995 Hyogo-Ken Nambu Earthquake," *Soils and Foundations*, **45**(5): 1–10.

Huang J, Zhao M, Xu C, *et al*. (2018), "Seismic Stability of Jointed Rock Slopes Under Obliquely Incident Earthquake Waves," *Earthquake Engineering and Engineering Vibration*, **17**(3): 527–539. https://doi.org/10.1007/s11803-018-0460-y

Koseki J, Bathurst RJ, Gu¨ler E, Kuwano J and Maugeri M (2006), "Seismic Stability of Reinforced Soil Walls," *Proceedings of the 8th International Conference on Geosynthetics*, Yokohama, Japan, pp. 51–78.

Krishna AM and Bhattacharjee A (2017), "Behavior of Rigid-Faced Reinforced Soil-Retaining Walls Subjected to Different Earthquake Ground Motions," *International Journal of Geomechanics*, **17**(1): 06016007. https://doi.org/10.1061/(ASCE)GM.1943-5622.0000668

Krishna AM and Bhattacharjee A (2019), "Seismic Analysis of Reinforced Soil Retaining Walls," *In Geotechnical Design and Practice*, pp. 159–171, Springer, Singapore. https://doi.org/10.1007/978-981-13-0505-4_14

Krishna AM and Latha GM (2007), "Seismic Response of Wrap-Faced Reinforced Soil-Retaining Wall Models Using Shaking Table Tests," *Geosynthetics International*, **14**(6): 355–364. DOI:10.1680/gein.2007.14.6.355

Latha GM and Krishna AM (2008), "Seismic Response of Reinforced Soil Retaining Wall Models: Influence of Backfill Relative Density," *Geotext Geomembr*, **26**(4): 335–349.

Lu X, Yang B and Zhao B (2018), "Shake-Table Testing of a Self-Centering Precast Reinforced Concrete Frame with Shear Walls," *Earthquake Engineering and Engineering Vibration*, **17**(2): 221–233. https://doi.org/10.1007/s11803-018-0436-y

Matsuo O, Tsutsumi T, Yokoyama K and Saito Y (1998), "Shaking Table Tests and Analyses of Geosynthetic-Reinforced Soil Retaining Walls," *Geosynthetics International*, **5**(1–2): 97–126. DOI:10.1680/gein.5.0116

Mohanty P, Xu D, Biswal S, *et al*. (2021), "A Shake Table Investigation of Dynamic Behavior of Pile Supported Bridges in Liquefiable Soil Deposits," *Earthquake Engineering and Engineering Vibration*, **20**: 1–24. https://doi.org/10.1007/s11803-021-2002-2

Murata O, Tateyama M and Tatsuoka F (1994), "Shaking Table Testson a Large Geosynthetic-Reinforced Soil Retaining Wallmodel," In: Tatsuoka F, Leshchinsky D (eds), *Recent Casehistories of Permanent Geosynthetic-Reinforced Soilretaining Walls*, Balkema, Rotterdam, pp. 259–264.

Nova-Roessig L and Sitar N (2006), "Centrifuge Model Dtudies of the Seismic Response of Reinforced Soil Slopes," *Journal of Geotechnical and Environmental Engineering*, **132**(3): 388–400. DOI:10.1061/(ASCE)1090-0241(2006)132:3(388)

Pan P, Gou YM, Kang YJ, Wang T and Han QH (2022), "Development of a Double-Layer Shaking Table for Large-Displacement High-Frequency Excitation," *Earthquake Engineering and Engineering Vibration*,

21(1): 193–207. https://doi.org/10.1007/s11803-022-2080-9

Perez A and Holtz RD (2004), "Seismic Response of Reinforced Steep Soil Slopes: Results of a Shaking Table Study," *Geotechnical Engineering for Transportation Projects*, ASCE Geotechnical Special Publication ASCE, Reston, VA, USA, **126**: 1664–1672. DOI: 10.1061/40744(154)159

Sabermahandi M, Ghalandarzadeh A and Fakher A (2009), "Experimental Study on Seismic Deformation Modes of Reinforced-Soil Walls," *Geotextiles and Geomembranes*, **27**(2): 121–136. https://doi.org/10.1016/j.geotexmem.2008.09.009

Sakaguchi M (1996), "A Study of the Seismic Behavior of Geosynthetic Reinforced Walls in Japan," *Geosynthetics International*, **3**(1): 13–30. https://doi.org/10.1680/gein.3.0051

Sakaguchi M, Muramatsu M and Nagura K (1992), "A Discussion Onreinforced Embankment Structures Having High Earthquakeresistance," *In: Proceedings of the International Symposiumon Earth Reinforcement Practice*, IS-Kyushu′92, Fukuoka, Japan, **1**: 287–292.

Telekes G, Sugimoto M and Agawa S (1994), "Shaking Table Tests Onreinforced Embankment Models," *In: Proceedings of the 13th International Conference on Soil Mechanics and Foundation Engineering*, New Delhi, India, **2**: 649–654.

Turan A, Hinchberger SD and El Naggar H (2009), "Design and Commissioning of a Laminar Soil Container for Use on Small Shaking Tables," *Soil Dynamics and Earthquake Engineering*, **29**(2): 404–414. doi:10.1016/j.soildyn.2008.04.003

Viswanadham BVS, Phanikumar BR and Mukherjee RV (2009), "Swelling Behaviour of a Geofiber-Reinforced Expansive Soil," *Geotextiles and Geomembranes*, **27**(1): 73–76. doi:10.1016/j.geotexmem.2008.06.002

Wang L, Chen G and Chen S (2015), "Experimental Study on Seismic Response of Geogrid Reinforced Rigid Retaining Walls with Saturated Backfill Sand," *Geotextiles and Geomembranes*, **43**: 35–45.

Washida S and Shimazu T (1988), "Seismic Resistance of Reinforced Embankment by Model Shaking Table Tests," *In: Proceedings of the International Geotechnical Symposium on Theory and Practice of Earth Reinforcement*, Fukuoka, Japan, pp. 413–418.

Wulandari SP and Tjandra D (2015), "Analysis of Geotextile Reinforced Road Embankment Using PLAXIS 2D", *Procedia Engineering*, **125**: 358–362.

Yegian MK, Kadakal U and Catan M (1999), "Geosynthetics for Earthquake Hazard Mitigation," In: *Geosynthetics 99*: *Specifying Geosynthetics and Developing Design Details*. **1**: 87–100.

Zhang J, Li YR, Zhixiao Yan ZX, Huang D, Rong X and Liang Y (2022), "Experimental Study of Vertical and Batter Pile Groups in Saturated Sand Using a Centrifuge Shaking Table," *Earthquake Engineering and Engineering Vibration*, **21**(1): 23–36. https://doi.org/10.1007/s11803-021-2067-y

Zhou Z, Gao YF, Zhang F, Song J and Zou D (2020), Effects of Soil Dynamic Response on Post-Earthquake Deformation of Slopes Based on Nested Newmark Model," *Earthquake Engineering and Engineering Vibration*, **19**(3): 573–582. https://doi.org/10.1007/s11803-020-0581-y